

Mode Shape Corrections for Wind Load Effects

Yin Zhou¹; Ahsan Kareem, M.ASCE²; and Ming Gu, M.ASCE³

Abstract: Traditionally, wind analysis procedures based on the “gust loading factor” approach and experimental techniques involving the high frequency base balance and the “stick-type” aeroelastic model test have assumed ideal structural mode shapes, i.e., linear lateral modes and uniform torsional modes. The influence of nonideal mode shapes manifests itself through modifications in the generalized wind load, the structural displacement, the equivalent static wind load (ESWL), and the attendant influence function. This has led to the introduction of several correction procedures, each focusing on an individual feature of the overall response analysis framework. This paper presents a systematic development of correction procedures in terms of correction factors (CFs) to account for nonideal mode shapes in the formulation of generalized load, analysis of structural response, and the derivation of the ESWL. A parameter study is conducted to examine the significance of CFs in estimating various load effects. It is observed that the influence of a nonideal mode shape is actually negligible for the displacement response and the base bending moment, but not so for other load effects, e.g., the base shear and the generalized wind load. Although the existing procedures are effective in correcting the intended response component, they should not be used indiscriminately for other load effects. This paper also presents a correction procedure for the influence of mode shapes on the ESWLs, a loading format that is very attractive for implementation in codes and standards and design practice as well as for the correct interpretation of wind tunnel measurements.

DOI: 10.1061/(ASCE)0733-9399(2002)128:1(15)

CE Database keywords: Wind loads; Shape; Wind analysis.

Introduction

Throughout the development of current analysis procedures such as the “gust loading factor” (GLF) method (Davenport 1967) and experimental techniques involving the high frequency base balance (HFBB) and the “stick” type aeroelastic model test, ideal structural mode shapes, i.e., linear lateral modes and uniform torsion modes, have traditionally been assumed. Correspondingly, these analysis procedures and experimental techniques work best for structures having exactly that ideal mode shape. However, most structures may exhibit a departure from these ideal mode shapes. Correction procedures are thus needed to consider the influence of nonideal mode shapes on the measured or calculated load effects. In this context, several correction procedures have been developed in the last few decades, each focusing on a particular aspect of the overall response analysis framework.

A correction formula for the GLF was given by Vickery (1970) in which the error for the actual mode shape deviating from a straight line was found to be within 1–3%. A similar observation was made by Tamura et al. (1996). In light of this, the effect of a

nonlinear mode shape has been excluded in the GLF-based analysis procedures given in major codes and standards (e.g., AS 1989; AIJ 1993). However, as pointed out by Zhou et al. (1999b), the traditional GLF is essentially the gust factor for the first mode displacement. The correction for the GLF in this context only reflects the effect of mode shape on the displacement response, which is negligible. However, since the effect of a nonlinear mode shape on other response components may not be as small as that on the displacement, disregarding this effect may lead to unrealistic estimates of the other response components.

Vickery’s finding (Vickery 1970) was also utilized by several investigators in the early development of the HFBB technique. Tschanz and Davenport (1983) identified a need to correct the torsional component measured using the HFBB. They suggested an approximate correction based on the base shear component measured by the balance. Kareem (1990) compared the torsional loads using an HFBB and multiple-point simultaneous pressure measurements and highlighted the need for corrections to HFBB measurements. The HFBB technique uses the measured base bending or torsional moments on structural models to represent the generalized wind loads acting on the actual building. As this approach gained greater acceptance, several mode shape correction procedures were proposed regarding the generalized wind load (e.g., Kareem 1984; Kijewski and Kareem 1998; Ho et al. 1999). Based on experimental data, Tallin and Ellingwood (1985) suggested a conservative correction factor (CF) of 2/3 for the generalized torsional moment. Similar values have been suggested by Holmes (1987) and Xu and Kowk (1993).

Vickery et al. (1985) noted that the influence of mode shape on the base bending moment and the acceleration are different from the influence on the generalized wind load. However, no correction procedure was offered. Recognizing that the generalized wind load is arbitrary in magnitude, Boggs and Peterka

¹Postdoctoral Research Associate, Dept. of Civil Engineering and Geological Science, NatHaz Modeling Laboratory, Univ. of Notre Dame, Notre Dame, IN 46556.

²Robert M. Moran Professor and Chair, Dept. of Civil Engineering and Geological Science, Univ. of Notre Dame, Notre Dame, IN 46556

³Professor, Dept. of Bridge Engineering, Tongji Univ., Shanghai 200092, People’s Republic of China.

Note. Associate Editor: James L. Beck. Discussion open until June 1, 2002. Separate discussions must be submitted for individual papers. To extend the closing date by one month, a written request must be filed with the ASCE Managing Editor. The manuscript for this paper was submitted for review and possible publication on July 7, 2000; approved on March 12, 2001. This paper is part of the *Journal of Engineering Mechanics*, Vol. 128, No. 1, January 1, 2002. ©ASCE, ISSN 0733-9399/2002/1-15–23/\$8.00+\$0.50 per page.

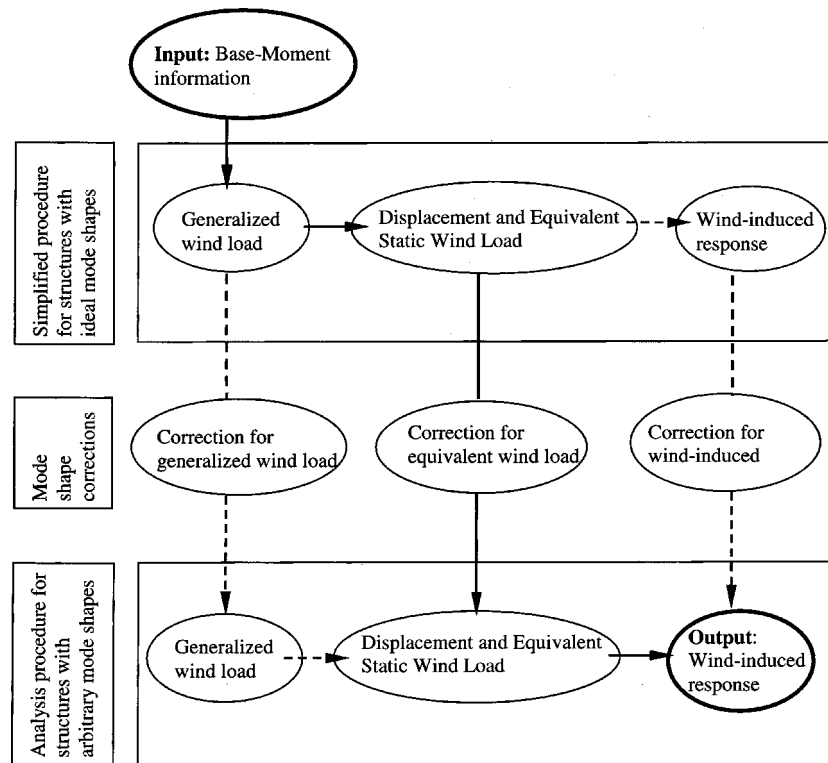


Fig. 1. Mode shape correction schemes

(1989) suggested that the mode shape correction should be applied to actual quantities rather than the generalized quantities. They introduced a load correction factor, which is essentially related to the base bending moment. However, because the base moment factor is not so sensitive to the mode shape, as will be demonstrated in the paper, care must be exercised in using this CF to wind load effects other than the base bending moment.

The Australian Standards, AS1170.2 (1989), provides two correction factors $(1.06 - 0.06\beta)$ ($\beta =$ exponent of the first mode shape) and $(0.76 + 0.24\beta)$ for adjusting the across-wind base bending moment and the acceleration response, respectively. Similarly, the Architectural Institute of Japan standard (AIJ 1993), provides $(0.73 + 0.27\beta)$ as a correction for displacement.

In this paper the effect of nonideal mode shapes is examined in the overall analysis framework for the wind-induced response. Two formulations for the wind-induced response, one based on arbitrary nonideal mode shapes and the second involving ideal mode shapes, are derived. Through a comparison between these two formulations, mode shape CFs are evaluated at each step of the overall analysis procedure for a range of wind-induced response components. A parameter study is carried out to delineate the influence of the mode shape exponent, mass distribution, wind pressure correlation, and the wind profile on the CFs. The results are discussed and compared with those reported in the literature. Since the CFs presented here are dependent on the response component of interest, a correction procedure for a wider range of applications is presented in terms of the equivalent static wind load (ESWL). For the sake of illustration, the overall scheme of the correction procedure for generalized load, ESWL, and associated response in the overall analysis framework is highlighted in Fig. 1.

Analysis of Wind-Induced Response

Arbitrary Nonideal Mode Shapes

In this paper a subscript X is used to represent the lateral mode and Z the torsion mode. If not specified particularly, the formulation would be applicable to both the lateral and the torsion modes. It is noted that for wind-induced response of most buildings based on convenient HFBB, the resonant response in modes higher than the first is neglected (Reinhold and Kareem 1986), although for acceleration response, among others, this assumption may not be very conservative (Kareem 1981). This paper also assumes that there is no modal coupling between the three fundamental structural modes. For cases in which modal coupling exists, problem-specific mode shape corrections may be sought. Alternatively, simultaneously measured multiple-point surface pressure at strategically located taps can provide mapping of the pressure field which can be weighted according to the mode shapes (Kareem 1982a; ASCE 1999). In situations where the modal coupling is deemed to amplify the load effects, a multi-degree-of-freedom aeroelastic model may be the method of choice.

The wind-induced response of a structure in the fundamental lateral mode is given by

$$m^* \ddot{\xi}(t) + c^* \dot{\xi}(t) + k^* \xi(t) = P^*(t) \quad (1)$$

where ξ , $m^* = \int_0^H m(z) \varphi^2(z) dz$; $c^* = 2\zeta \sqrt{k^* m^*}$, $k^* = (2\pi f_1)^2 m^*$, and $P^*(t) = \int_0^H P(z, t) \varphi(z) dz =$ generalized displacement, mass, damping, stiffness, and externally applied wind loading in the first mode, respectively; $\zeta = \zeta_A + \zeta_S$, in which ζ , ζ_S , and $\zeta_A =$ total, structural, and aerodynamic damping ratios, respectively; $f_1 =$ natural frequency of the first mode; $m(z) =$ mass distribution, which may be assumed to be linearly distrib-

uted for tall structures as $m(z) = m_0[1 - \lambda(z/H)]$ where $\lambda = (m_0 - m_H)/m_0$, the “mass reduction factor” (Boggs and Peterka 1989); m_0 and m_H = mass per unit height evaluated at the bottom and the top of the building, respectively; and the first structural mode shape may be approximated by $\varphi(z) = c_1(z/H)^\beta$ where c_1 = normalization factor. A similar expression can be written for the torsional response.

The RMS generalized displacement response in the first mode is given by

$$\sigma_\xi = \frac{1}{k^*} \left(\int_0^\infty |H(f)|^2 S_{P^*}(f) df \right)^{1/2} \quad (2)$$

where $|H(f)|^2 = \{[1 - (f/f_1)^2]^2 + (2\xi f/f_1)^2\}^{-1}$ = structural transfer function; and

$$S_{P^*}(f) = \int_0^H \int_0^H P(z_1)P(z_2)S_p(f)Q(z_1, z_2, f) \cdot \varphi(z_1)\varphi(z_2)dz_1dz_2 \quad (3)$$

is the generalized wind load, in which $S_p(f)$ = unit fluctuating wind force or torque spectrum; $P(z) = P_H(z/H)^\gamma$, where P_H = amplitude of the fluctuating wind force evaluated at the building top; γ = fluctuating wind profile exponent; and $Q(z_1, z_2, f) = \exp(-C_K f/\bar{V} \cdot |z_1 - z_2|/H)$ = coherence of the fluctuating wind pressures, in which \bar{V} = reference mean wind velocity and C_K = an exponential decay coefficient.

The wind-induced response is customarily divided into the resonant and the background components. The former is dominant in the case of flexible structures and the latter for relatively stiffer structures. Taking the resonant component as an example, the displacement response in the first mode can be computed by

$$\begin{aligned} \sigma_{DR}(z) &= \sigma_{\xi R} \cdot \varphi(z) \\ &= \frac{P_H}{(2\pi f_1)^2 H m_0} \cdot \frac{(1+2\beta)(2+2\beta)}{[(2+2\beta) - \lambda(1+2\beta)]} \\ &\quad \cdot \sqrt{|J(\gamma, \beta, f_1)|^2 \frac{\pi f_1}{4\xi} S_p(f_1)} \left(\frac{z}{H} \right)^\beta \end{aligned} \quad (4)$$

where $|J(\gamma, \beta, f)|^2 = \int_0^H \int_0^H (z_1/H)^\gamma + \beta (z_2/H)^\gamma + \beta Q(z_1, z_2, f) \times dz_1 dz_2$ is usually referred to as the joint acceptance function (Davenport 1967) and the subscript D denotes the displacement response.

Although the wind-induced displacement is an important quantity, information concerning other response components, e.g., the internal forces in individual structural members, are needed for design. The ESWL facilitates convenient assessment of other response components. Utilizing the resonant displacement response, the resonant component of the RMS ESWL can be represented in terms of the inertial load

$$\begin{aligned} \sigma_{FR}(z) &= m(z) \cdot (2\pi f_1)^2 \cdot \sigma_{DR}(z) \\ &= \frac{P_H(1+2\beta)(2+2\beta)}{H[(2+2\beta) - \lambda(1+2\beta)]} \cdot \sqrt{|J(\gamma, \beta, f_1)|^2 \frac{\pi f_1}{4\xi} S_p(f_1)} \\ &\quad \times \left(1 - \lambda \frac{z}{H} \right) \left(\frac{z}{H} \right)^\beta \end{aligned} \quad (5)$$

where the subscript F indicates the ESWL. Note that the distribution of the displacement follows the mode shape, while the ESWL depends on both the mode shape and the mass distributions.

One of the attractive features of the ESWL formulation is that

any desired wind-induced response can be obtained through a simple static analysis by introducing an appropriate influence function. In fact, the RMS response due to resonant effects can be given by

$$\begin{aligned} \sigma_{rR} &= \int_0^H \sigma_{FR}(z) i(z) dz \\ &= \frac{P_H i_c \cdot (1+2\beta)(2+2\beta)}{[(2+2\beta) - \lambda(1+2\beta)]} \cdot \frac{[(2+\beta+\beta_0) - \lambda(1+\beta+\beta_0)]}{(2+\beta+\beta_0) \cdot (1+\beta+\beta_0)} \\ &\quad \times \sqrt{|J(\gamma, \beta, f_1)|^2 \frac{\pi f_1}{4\xi} S_p(f_1)} \end{aligned} \quad (6)$$

where the subscript r refers to an arbitrary response relevant to an influence function, which is expressed by

$$i(z) = i_c (z/H)^{\beta_0} \quad (7)$$

where i_c and β_0 are both constants. For the base shear force and base moment in the lateral mode, these coefficients are $i_c = 1$, $\beta_0 = 0$, and $i_c = H$, $\beta_0 = 1$, respectively; for the base torque, $i_c = 1$, $\beta_0 = 0$; and for the displacement, $\beta_0 = \beta$.

The background response can be derived using the influence function in a more straightforward manner (Zhou et al. 2000)

$$\begin{aligned} \sigma_{rB} &= \left(\int_0^\infty \int_0^H \int_0^H P(z_1)P(z_2)S_p(f)Q(z_1, z_2, f) \right. \\ &\quad \left. \cdot i(z_1)i(z_2)dz_1dz_2df \right)^{1/2} \\ &= P_H i_c \cdot \left(\int_0^\infty S_p(f) |J(\gamma, \beta_0, f)|^2 df \right)^{1/2} \end{aligned} \quad (8)$$

Note that the background response given in Eq. (8) includes the contributions from all the higher modes and coupling among modes. The corresponding background ESWL can be derived using the “Load-Response-Correlation” approach (Kasperski and Niemann 1992). Usually, its distribution is dependent on the response of interest and differs from the distribution of the resonant ESWL components (Zhou et al. 2000).

The resultant peak response can be obtained using an SRSS combination rule

$$\hat{r} = \bar{r} + \sqrt{(g_B \sigma_{rB})^2 + (g_R \sigma_{rR})^2} \quad (9)$$

in which \hat{r} = peak resultant response; \bar{r} = mean response; and g_B and g_R = background and resonant peak factors, respectively.

Simplified Analysis with Ideal Mode Shapes

While the analysis procedures in the preceding section are accurate, they can only give meaningful solutions in a limited number of situations. These situations include those where experimental measurements are available to evaluate the aerodynamic pressure distributions and their complementary correlation structure (Kareem 1982b) or where quasi-steady and strip theories are applicable for buffeting analysis. However, in engineering applications, such complete information about the aerodynamic loads is not always available.

On the other hand, when a building has an ideal mode shape, i.e., linear lateral mode shape and uniform torsional mode shape, simplified analysis procedures can be derived from the preceding formulation. For example, considering a linear lateral mode shape

($\beta = 1.0$), the PSD of the generalized wind loads can be conveniently determined by

$$S_{p_x^*}(f) = S_{M_X}(f)/H^2 \quad (10)$$

in which $S_{M_X}(f)$ = PSD of the aerodynamic base bending moment. The relationship in Eq. (10) has led to the popularity of the HFBB technique in which the spectrum of the measured base moment on the scaled building model is proportional to the linear mode generalized wind load spectrum on the actual building.

Given the generalized wind load, the wind-induced response can be computed. For example, the RMS displacement in the lateral mode is given by

$$\sigma'_{DX}(z) = \frac{1}{(2\pi f_1)^2 \int_0^H m(z)(z/H)^2 dz} \cdot \left(\int_0^\infty |H(f)|^2 \cdot S_{M_X}(f)/H^2 \cdot df \right)^{1/2} \cdot (z/H) \quad (11)$$

where the prime denotes results based on the ideal mode shape. Other wind load effects, such as the ESWL and wind-induced response, can also be expressed in terms of the aerodynamic base moments. These quantities are given in the Appendix for further comparison. It is noteworthy that in the simplified formulation the displacement increases linearly along the height in the lateral mode and uniformly in the torsional mode. The distribution of the ESWL is a function of the ideal mode shape and the mass distributions as shown in Eqs. (28)–(35) of the Appendix.

Mode Shape Corrections

In this section, mode shape corrections for the generalized wind loads, wind-induced response, and the equivalent static wind loads are presented.

Generalized Wind Loads

HFBB tests provide the generalized wind load on structures with the implicit assumption of an ideal mode shape. For the lateral response, when the mode shape of an actual building deviates from a straight line, the following mode shape correction has been introduced to correct the base bending moment to obtain the generalized wind loads (e.g., Xu and Kowk 1994; Kijewski and Kareem 1998):

$$\phi_X(\beta) = \frac{\sigma_{p_x^*}(\beta)}{\sigma'_{p_x^*}} = \frac{\sigma_{p_x^*}(\beta)}{\sigma_{M_X}/H} \quad (12)$$

where $\sigma_{p_x^*}(\beta)$ and $\sigma'_{p_x^*}$ = RMS generalized wind loads for arbitrary and ideal mode shapes, respectively. Using Eqs. (3) and (12), this CF can be derived

$$\phi_X(\beta) = \sqrt{\frac{\int_0^\infty |J(\gamma, \beta, f)|^2 S_p(f) df}{\int_0^\infty |J(\gamma, 1, f)|^2 S_p(f) df}} \quad (13)$$

Utilizing the measured aerodynamic base bending moment in conjunction with the CF for the generalized wind load, the wind-induced response, for example, the displacement in Eq. (4), can then be computed by

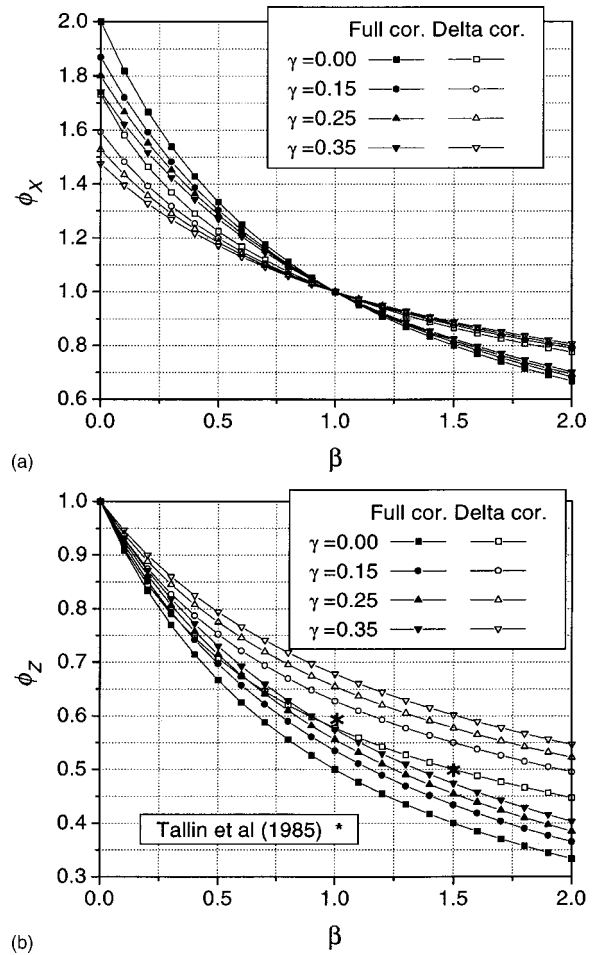


Fig. 2. Mode shape corrections for generalized wind loads: (a) lateral mode [Eq. (13)] and (b) torsion mode [Eq. (15)]

$$\sigma_{DX}(z) = \frac{1}{(2\pi f_1)^2 \int_0^H m(z)\phi^2(z) dz} \cdot \left(\int_0^\infty |H(f)|^2 \cdot \phi_X(\beta)^2 \cdot S_{M_X}(f)/H^2 df \right)^{1/2} \cdot \phi(z) \quad (14)$$

Similarly, the CF for the generalized wind load in torsion is given by

$$\phi_Z(\beta) = \sqrt{\frac{\int_0^\infty |J(\gamma, \beta, f)|^2 S_p(f) df}{\int_0^\infty |J(\gamma, 0, f)|^2 S_p(f) df}} \quad (15)$$

The variation in the CFs for the generalized wind loads in terms of mode shape exponents and other involved parameters is shown in Fig. 2. As expected, when the mode shape is ideal, i.e., $\beta = 1$ for lateral mode or $\beta = 0$ for the torsional mode, the CFs have unit values regardless of other parameters. However, significant corrections are needed when the actual mode shapes deviate from this assumption since the CFs for both lateral and torsional modes are dependent on the mode shape exponents. The CFs are insensitive to the wind profile exponent for $\gamma = 0-0.35$. For two limiting correlation cases, i.e., full correlation ($C_K = 0$) and zero correlation ($C_K \rightarrow \infty$), the effect of the correlation on CFs in the

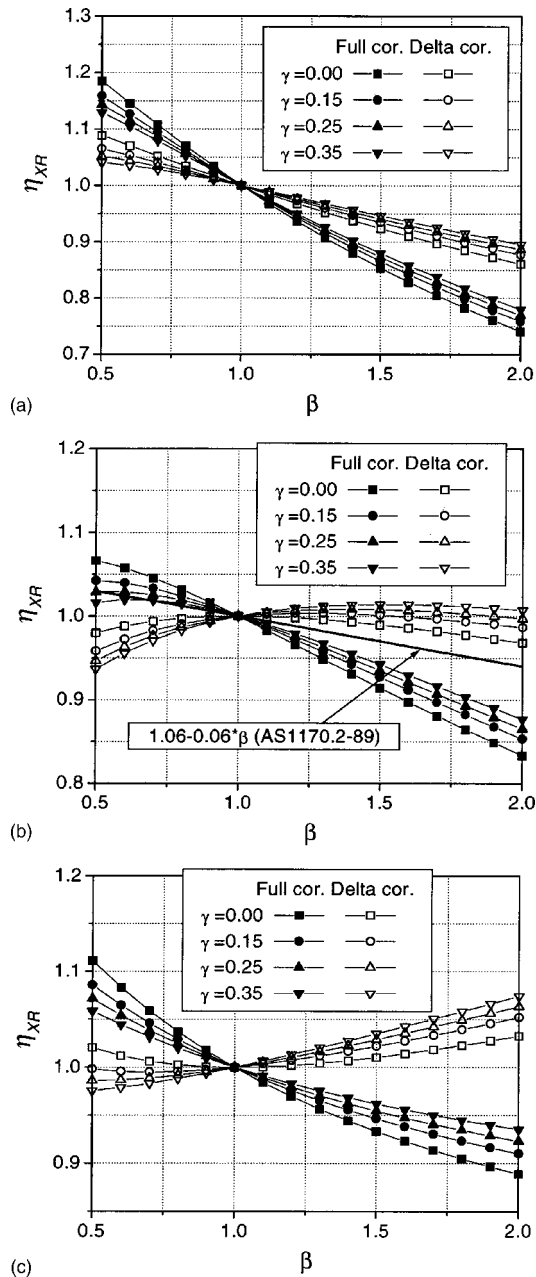


Fig. 3. Mode shape corrections for resonant response in lateral mode [Eq. (16)]: (a) base shear and (b) base bending moment; (c) first mode displacement

lateral and torsional modes are within 10% and 15%, respectively. The CFs are less than unity for the lateral mode when $\beta > 1$ and for the torsion when $\beta > 0$. This means a direct use of the measured aerodynamic load without mode shape modification will lead to conservative estimates of wind-induced response. Based on experimental data, a CF equal to $2/3$ (Tallin and Ellingwood 1985) or 0.7 (Vickery et al. 1985) has been suggested, which is widely used in wind tunnel testing. However, as noted in Fig. 2(b), this value may not be accurate for a wide range of mode shapes.

Although the mode shape correction for the generalized wind load has been most widely used in research, some inherent shortcomings relevant to this concept still call for special attention. The first is related to the definition of this correction. The generalized wind load is arbitrary in magnitude depending on the nor-

malization factor of the mode shape, c_1 , while the base moment is a unique quantity. Therefore the correction for the generalized wind load in Eq. (12) is, strictly speaking, arbitrary in magnitude. This problem can be eliminated by setting $c_1 = 1$. However, it may be sometimes in disagreement with the mode shape normalization scheme employed by the end-user. The second shortcoming concerns the correct use of this CF in wind-induced response analysis procedures. As given in Eq. (14), an actual mode shape, rather than an ideal mode shape, should be used for the generalized mass and the displacement distributions. A misrepresentation of the mode shape in Eq. (14) and in the follow-up procedure may significantly impact the final results (Vickery et al. 1985).

Wind-Induced Response

Following the mode shape correction for the generalized wind load, which is actually the ratio between the actual generalized wind load and that based on an ideal mode shape, the mode shape correction for the wind-induced response can be formulated. The mode shape correction is addressed separately here for the resonant and the background components.

Resonant Response

The CF for the resonant response is defined as the ratio between the resonant response of the actual structure and that obtained using the idealized modes. Referring to Eqs. (6), (31), and (35), the CFs for the lateral and the torsional modes are given by

$$\begin{aligned} \eta_{rXR} &= \frac{\sigma_{rXR}}{\sigma'_{rXR}} \\ &= \frac{(4-3\lambda) \cdot (1+2\beta)(2+2\beta)}{12[(2+2\beta)-\lambda(1+2\beta)]} \\ &\quad \times \frac{(3+\beta_0)(2+\beta_0) \cdot [(2+\beta+\beta_0)-\lambda(1+\beta+\beta_0)]}{(2+\beta+\beta_0)(1+\beta+\beta_0) \cdot [(3+\beta_0)-\lambda(2+\beta_0)]} \\ &\quad \times \sqrt{\frac{|J(\gamma, \beta, f_1)|^2}{|J(\gamma, 1, f_1)|^2}} \end{aligned} \quad (16)$$

$$\begin{aligned} \eta_{rZR} &= \frac{\sigma_{rZR}}{\sigma'_{rZR}} \\ &= \frac{(2-\lambda) \cdot (1+2\beta)(2+2\beta)}{2[(2+2\beta)-\lambda(1+2\beta)]} \\ &\quad \times \frac{(2+\beta_0)(1+\beta_0) \cdot [(2+\beta+\beta_0)-\lambda(1+\beta+\beta_0)]}{(2+\beta+\beta_0)(1+\beta+\beta_0) \cdot [(2+\beta_0)-\lambda(1+\beta_0)]} \\ &\quad \times \sqrt{\frac{|J(\gamma, \beta, f_1)|^2}{|J(\gamma, 0, f_1)|^2}} \end{aligned} \quad (17)$$

It is noted that the CFs in Eqs. (16) and (17) are dependent not only on the exponent γ , the correlation of the externally applied aerodynamic loads Q , and the dynamic characteristics of the structure β , but also on the response component of interest β_0 . Also, as expected for ideal mode shapes, both CFs are unity regardless of other parameters. For the lateral mode, employing a full correlation and substituting $\beta_0 = 1$ in Eq. (16) will result in the CF alluded to in Boggs and Peterka (1989) as the load factor. Obviously, this CF is different from that of the base shear, which can be obtained by substituting $\beta_0 = 0$. Similarly, the displacement CF can be obtained by substituting $\beta_0 = \beta$.

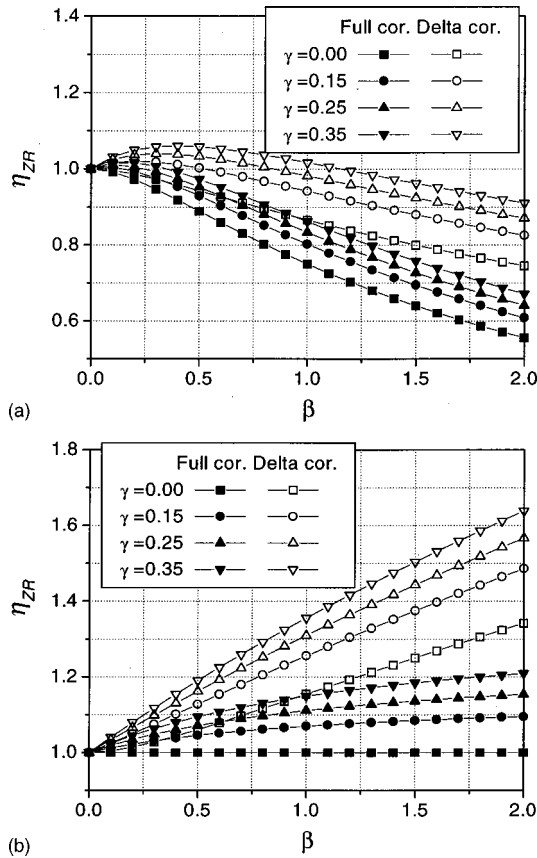


Fig. 4. Mode shape corrections for resonant response in torsion mode [Eq. (17)]: (a) base torque and (b) first mode deflection

For the sake of comparison with the findings reported in the literature, a uniform distribution of mass or mass moment of inertia is assumed in the parametric study. The CF for the resonant response in the lateral mode is plotted in Fig. 3. Note that when considering the limiting correlation condition, the CF is independent of the first mode frequency f_1 . The CF for the base shear force in Fig. 3(a) varies in the range of 0.75–1.18 for $\beta = 0.5$ –2.0. Therefore this mode shape correction cannot simply be neglected. Fig. 3(b) shows the base bending moment CF, which ranges from 0.84 to 1.06. The base moment CF provided in AS1170.2-89 is also shown in Fig. 3(b), which falls at the average value of the data for the two limiting correlation conditions. The displacement CF is plotted in Fig. 3(c), which varies in the range of 0.9–1.1 for $\beta = 0.5$ –2.0. For the along-wind displacement response, using the decay coefficients given in major codes, this factor deviates usually within 5% from unity. This reconfirms the findings of several researchers that the mode shape correction for the GLF is negligible (Vickery 1970; Tamura et al. 1996; Zhou et al. 1999a).

The CFs for the resonant torsional response are plotted in Fig. 4. Comparing with the CFs for the lateral mode, the torsional CFs are relatively sensitive to all the parameters involved and vary over a wider range. Fig. 4(a) shows the CF for the base torque ($\beta_0 = 0$). It varies in the range of 0.55–1.07, while most of it is less than unity. The first mode torsional deflection CF is plotted in Fig. 4(b), which varies within 1–1.6. This opposite trend is believed to result from the different ESWLs in the preceding two formulations. For the torsional mode, this effect is especially noteworthy.

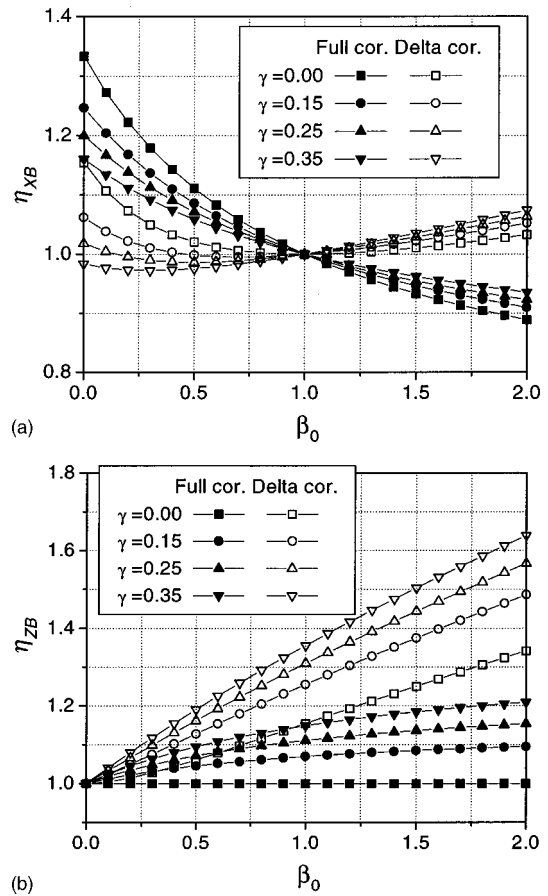


Fig. 5. Mode shape corrections for background response: (a) lateral mode [Eq. (18)] and (b) torsion mode [Eq. (19)]

Background Response

Like the resonant component, the CFs for the background response can be formulated in lateral and torsion modes by utilizing Eqs. (8), (31), and (35)

$$\eta_{rXB} = \frac{\sigma_{rXB}}{\sigma'_{rXB}} = \frac{(4-3\lambda) \cdot (3+\beta_0)(2+\beta_0)}{12 \cdot [(3+\beta_0) - \lambda(2+\beta_0)]} \cdot \sqrt{\frac{\int_0^\infty |J(\gamma, \beta_0, f)|^2 S_p(f) df}{\int_0^\infty |J(\gamma, 1, f)|^2 S_p(f) df}} \quad (18)$$

$$\eta_{rZB} = \frac{\sigma_{rZB}}{\sigma'_{rZB}} = \frac{(2-\lambda) \cdot (2+\beta_0)(1+\beta_0)}{2 \cdot [(2+\beta_0) - \lambda(1+\beta_0)]} \cdot \sqrt{\frac{\int_0^\infty |J(\gamma, \beta_0, f)|^2 S_p(f) df}{\int_0^\infty |J(\gamma, 0, f)|^2 S_p(f) df}} \quad (19)$$

Unlike the resonant response CFs, the background response CFs are independent of the dynamic characteristics of the structure, i.e., independent of β .

The background response CFs are plotted in Fig. 5. For the lateral mode, if $\beta_0 = 1$, then $\eta_{rXB} = 1$. This implies that the background base moment is equal to the base moment induced by the applied wind forces or can be scaled from the aerodynamic moment measured by the HFBB. This confirms the fact that the background response is quasi-steady in nature. However, the CFs for other background response components depart from unity as β_0 takes values other than unity. This is because the background response computed by the simplified formulation includes the contribution only from the fundamental mode, which may sometimes be insufficient. Taking the base shear as an example, the CF varies between 0.99 and 1.33. This correction is of significance for some relatively less flexible structures where the background response is normally predominant.

For the torsional mode, as shown in Fig. 5(b), the background base torque is also equal to the aerodynamic base torque ($\beta_0 = 0$). However, the CF is always greater than unity for other torsional background response components suggesting that the contribution resulting only from the fundamental mode is insufficient and should be used carefully.

Equivalent Static Wind Loads

Since the above mode shape corrections are all dependent on β_0 or the response component of interest, it may not be convenient to evaluate the CF for each desired response component in practice. To facilitate the use of CFs in design practice, a correction procedure for the ESWL is developed in this section. The advantage of the ESWL-based correction procedure is that the ESWL plays a unique role in design practice. With an accurate ESWL description, designers can obtain any wind-induced response component of interest with a simple static analysis, and no extra mode shape correction is needed.

Resonant ESWL Component

Comparing Eqs. (30) and (34) with Eq. (5) and assuming a uniform distribution of mass and mass moment of inertia as implied in most codes and standards, the ESWL on the actual structure for the lateral and torsion modes can be expressed by

$$\sigma_{FXR}(z) = \eta_{FXRH} \cdot \sigma'_{FXR}(H) \cdot (z/H)^\beta \quad (20)$$

$$\sigma_{FZR}(z) = \eta_{FZRH} \cdot \sigma'_{FZR}(H) \cdot (z/H)^\beta \quad (21)$$

where $\sigma'_{FXR}(H) = (3/H^2) \sqrt{\pi f_1 S_{MX}(f_1)/4\zeta}$ and $\sigma'_{FZR}(H) = (1/H) \sqrt{\pi f_1 S_{MZ}(f_1)/4\zeta}$ = resonant ESWL components evaluated at the top of the structure in the lateral and torsion modes, respectively, by referring to Eqs. (28), (30), (32), and (34) and setting $\lambda = 0$; and

$$\eta_{FXRH} = \frac{\sigma_{FXR}(H)}{\sigma'_{FXR}(H)} = \frac{(1+2\beta)}{3} \cdot \sqrt{\frac{|J(\gamma, \beta, f_1)|^2}{|J(\gamma, 1, f_1)|^2}} \quad (22)$$

$$\eta_{FZRH} = \frac{\sigma_{FZR}(H)}{\sigma'_{FZR}(H)} = (1+2\beta) \cdot \sqrt{\frac{|J(\gamma, \beta, f_1)|^2}{|J(\gamma, 0, f_1)|^2}} \quad (23)$$

are the CFs for the resonant ESWL components.

Fig. 6 shows the variation in the CFs for the resonant ESWL components. In the lateral mode, the correction factor η_{FXRH} is relatively insensitive to wind exponent and correlation parameters. As shown in Fig. 6(a), it can be approximated by

$$\eta_{FXRH} = 0.76 + 0.24 \times \beta \quad (24)$$

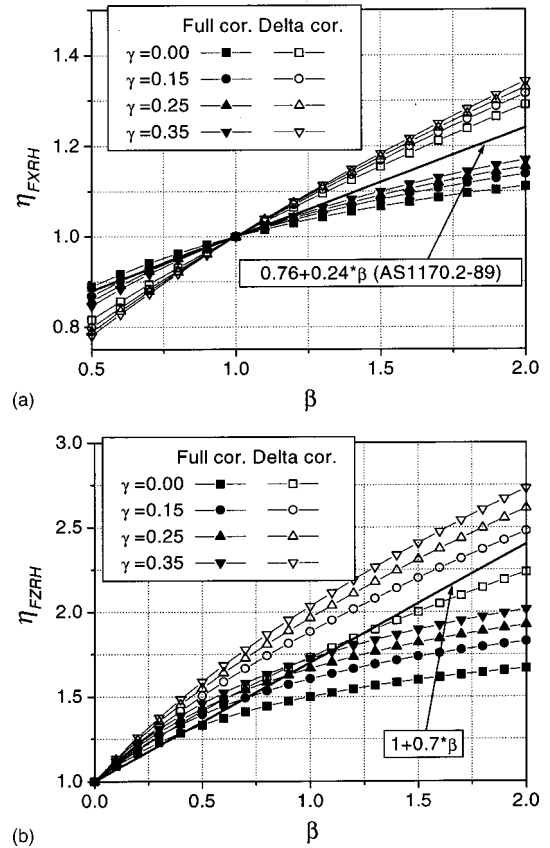


Fig. 6. Mode shape corrections for resonant equivalent static wind load components: (a) lateral mode [Eq. (22)] and (b) torsion mode [Eq. (23)]

This is the same as the acceleration CF suggested by AS1170.2 (1989), which introduces error within 10% for the two limiting correlation cases for $\beta = 0.5-2.0$. In Fig. 6(b) the torsion ESWL correction factor is relatively sensitive to wind parameters and can be approximated by

$$\eta_{FZRH} = 1.0 + 0.7 \times \beta \quad (25)$$

This introduces error within 30% for the two limiting correlation cases.

It is noteworthy that the above CF for the ESWL in the lateral mode can also be interpreted as the CF for the resonant displacement and acceleration evaluated at the top of the structure when assuming a uniform mass distribution. In fact, η_{FXRH} is consistent with the CFs used in AIJ-RLB (1993) and AS1170.2 (1989) for the displacement and the acceleration in the across-wind direction. However, the implication of the CF and its potential application to other load effects as given in Eq. (20) are not documented in these codes or their background documents. Meanwhile, it is also noted that the ESWL-based correction procedure is very useful to explain the experimental observations of the “stick-type” aeroelastic model test in which a displacement or an acceleration response is usually measured (Zhou and Kareem 2000).

Background ESWL Component

The following procedure is introduced for the background ESWL components

$$\sigma_{FXB}(z) = \frac{2+2\gamma}{H^2} \cdot \sigma_{MX} \cdot \left(\frac{z}{H}\right)^{2\gamma} \quad (26)$$

$$\sigma_{FZB}(z) = \frac{1+2\gamma}{H} \cdot \sigma_{MZ} \cdot \left(\frac{z}{H}\right)^{2\gamma} \quad (27)$$

in which σ_{MX} and σ_{MZ} = the RMS aerodynamic base bending moment and base torque measured by the HFBB or by other means. The first advantage of this procedure is that the wind loading is distributed according to the 2γ power law and it usually provides a reasonable representation of the background response component (Zhou et al. 1999b). The second advantage is that the background response can be simply obtained from the mean wind response by multiplying a background magnification factor because the wind load follows the distribution of the mean wind load in the lateral mode.

Concluding Remarks

Utilizing the high frequency base balance data, the wind-induced response of a structure with nonideal mode shapes can be obtained by means of mode shape correction factors (CFs). These CFs can be evaluated for different response components of interest by comparing the response of a structure with a nonideal mode shape to that with an ideal mode (Fig. 1). A parameter study shows that the influence of a nonideal mode shape is rather negligible for the structural displacement and the base bending moment, but not insignificant for other load effects such as the generalized wind loads, the base shear, and the acceleration response. This observation is consistent with comments made by earlier researchers. It is important to emphasize that although the existing correction procedures are effective in their own context, caution must be exercised in utilizing these procedures indiscriminately to estimate other load effects. In light of the overall

framework of the wind-induced response analysis, the existing correction procedures are particular cases of the overall general treatment presented in this paper. Among several mode shape correction schemes, the ESWL-based correction procedure offers a convenient framework for implementation in codes and standards and for providing correct interpretation of wind tunnel measurements. The procedures presented in this paper can be utilized immediately in the application of the HFBB measurements, the “stick-type” aeroelastic model tests, and the GLF approach.

Acknowledgments

The writers gratefully acknowledge the partial support from NSF Grants No. CMS 95-03779 and No. CMS 95-22145 for this study. The writers would also like to thank Dr. Xinzhong Chen, Dr. Fred L. Haan, Jr., and Tracy Kijewski for their comments on the manuscript.

Appendix: Wind Load Effects in Simplified Procedure

The PSD of the aerodynamic base bending moment in the lateral mode can be written as

$$\begin{aligned} S_{MX}(f) &= \int_0^H \int_0^H P(z_1)P(z_2)S_p(f)Q(z_1, z_2, f) \cdot z_1 z_2 dz_1 dz_2 \\ &= P_H^2 H^2 \cdot S_p(f) \cdot |J(\gamma, 1, f)|^2 \end{aligned} \quad (28)$$

Thus the RMS displacement, ESWL, and wind-induced response can be computed by

$$\sigma'_{DX}(z) = \frac{12 \cdot P_H}{(2\pi f_1)^2 H m_0 (4-3\lambda)} \sqrt{|J(\gamma, 1, f_1)|^2 \frac{\pi f_1}{4\zeta} S_p(f_1) + \int_0^\infty S_p(f) |J(\gamma, 1, f)|^2 df} \left(\frac{z}{H}\right) \quad (29)$$

$$\sigma'_{FX}(z) = \frac{12 P_H}{H(4-3\lambda)} \cdot \sqrt{|J(\gamma, 1, f_1)|^2 \frac{\pi f_1}{4\zeta} S_p(f_1) + \int_0^\infty S_p(f) |J(\gamma, 1, f)|^2 df} \left(1 - \lambda \frac{z}{H}\right) \left(\frac{z}{H}\right) \quad (30)$$

$$\sigma'_{rX} = \frac{12 \cdot P_H i_c [(3 + \beta_0) - \lambda(2 + \beta_0)]}{(4-3\lambda)(3 + \beta_0)(2 + \beta_0)} \sqrt{|J(\gamma, 1, f_1)|^2 \frac{\pi f_1}{4\zeta} S_p(f_1) + \int_0^\infty S_p(f) |J(\gamma, 1, f)|^2 df} \quad (31)$$

where the first item under the radical sign is the resonant component and the second is the background component.

For the torsional mode, these expressions are, respectively, given as follows

$$S_{MZ}(f) = \int_0^H \int_0^H P(z_1, f) P^*(z_2, f) dz_1 dz_2 = P_H^2 \cdot S_p(f) \cdot |J(\gamma, 0, f)|^2 \quad (32)$$

$$\sigma'_{DZ}(z) = \frac{2 P_H}{(2\pi f_1)^2 H m_0 \cdot (2-\lambda)} \cdot \sqrt{|J(\gamma, 0, f_1)|^2 \frac{\pi f_1}{4\zeta} S_p(f_1) + \int_0^\infty |J(\gamma, 0, f)|^2 S_p(f) df} \quad (33)$$

$$\sigma'_{rZ}(z) = \frac{2 \cdot P_H}{H(2-\lambda)} \cdot \sqrt{|J(\gamma, 0, f_1)|^2 \frac{\pi f_1}{4\zeta} S_p(f_1) + \int_0^\infty |J(\gamma, 0, f)|^2 S_p(f) df} \left(1 - \lambda \frac{z}{H}\right) \quad (34)$$

$$\sigma'_{rZ} = \frac{2 \cdot P_H i_c \cdot [(2 + \beta_0) - \lambda(1 + \beta_0)]}{(2-\lambda)(2 + \beta_0)(1 + \beta_0)} \cdot \sqrt{|J(\gamma, 0, f_1)|^2 \frac{\pi f_1}{4\zeta} S_p(f_1) + \int_0^\infty |J(\gamma, 0, f)|^2 S_p(f) df} \quad (35)$$

It is noted that in the practical application, the aerodynamic moments are directly measured using HFBB and other tools. The above expressions can correspondingly be rewritten by using the measured moments as the input.

References

- American Society of Civil Engineers (ASCE). (1999). *Wind Tunnel Studies of Buildings and Structures, ASCE Manuals and Reports on Engineering Practice No. 67*, Reston, Va.
- Architectural Institute of Japan (AIJ). (1993). *Recommendations for Loads on Buildings*, Tokyo (in Japanese).
- Australian Standards (AS). (1989). "SAA Loading code, part 2-wind forces." AS1170.2-89, Sydney, Australia.
- Boggs, D. W., and Peterka, J. A. (1989). "Aerodynamic model tests of tall buildings." *J. Eng. Mech.*, 115(3), 618–635.
- Davenport, A. G. (1967). "Gust loading factors." *J. Struct. Div. ASCE*, 93(3), 11–34.
- Holmes, J. D. (1987). "Mode shape corrections for dynamic response to wind." *Eng. Struct.*, 9, 210–212.
- Kareem, A. (1981). "Wind excited response on buildings in higher modes." *J. Struct. Eng.*, 107(4), 701–706.
- Kareem, A. (1982a). "Measurements of total dynamic loads from surface pressures." *Proc., Int. Workshop on Wind Tunnel Modeling Criteria and Techniques*, National Bureau of Standards, Gaithersburg, Md., Cambridge University Press.
- Kareem, A. (1982b). "Fluctuating wind loads on buildings." *J. Eng. Mech. Div.*, 108(6), 1086–1102.
- Kareem, A. (1984). "Model for prediction of the across-wind response of buildings." *Eng. Struct.*, 6(2), 136–141.
- Kareem, A. (1990). "Measurements of pressure and force fields on building models in simulated atmospheric flows." *J. Wind Eng. Indust. Aerodyn.*, 36, 589–599.
- Kasperski, M., and Niemann, H. J. (1992). "The L.R.C. method—a general method of estimating unfavorable wind load distributions for linear and non-linear structures." *J. Wind Eng. Indust. Aerodyn.*, 41–44, 1753–1763.
- Kijewski, T., and Kareem, A. (1998). "Dynamic wind effects: a comparative study of provisions in codes and standards with wind tunnel data." *Wind Struct.*, 1(1), 77–109.
- Reinhold, T. A., and Kareem, A. (1986). "Wind loads and building response predictions using force-balance techniques." *Proc., 3rd ASCE Engineering Mech. Conf.—Dynamics of Structures*, Univ. of California, Los Angeles.
- Tallin, A., and Ellingwood, B. (1985). "Analysis of torsional moments on tall buildings." *J. Wind Eng. Indust. Aerodyn.*, 18, 191–195.
- Tschanz, T., and Davenport, A. G. (1983). "The base balance technique for the determination of dynamic wind loads." *J. Wind Eng. Indust. Aerodyn.*, 13, 429–439.
- Vickery, B. J. (1970). "On the reliability of gust loading factors." *Proc., Technical Meeting Concerning Wind Loads on Buildings and Structures*, Building Science Series 30, National Bureau of Standards, Washington, D.C., 296–312.
- Vickery, P. J., Steckley, A. C., Isyumov, N., and Vickery, B. J. (1985). "The effect of mode shape on the wind-induced response of tall buildings." *Proc., 5th U.S. National Conf. on Wind Engineering*, Texas Technical Univ., Lubbock, Tex.
- Xu, Y. L., and Kowk, K. C. S. (1993). "Mode shape corrections for wind tunnel tests of tall buildings." *Eng. Struct.*, 15(5), 387–392.
- Zhou, Y., Gu, M., and Xiang, H. F. (1999a). "Along-wind static equivalent wind loads and response of tall buildings Part II: effects of mode shapes." *J. Wind Eng. Indust. Aerodyn.*, 79(1,2), 151–158.
- Zhou, Y., and Kareem, A. (2000). "Aeroelastic Balance." *Proc., 4th Int. Colloquium on Bluff Body Aerodynamics and Applications*, Bochum, Germany, 599–602.
- Zhou, Y., Kareem, A., and Gu, M. (1999b). "Gust loading factors for design applications." *Proc., 10th Int. Conf. on Wind Engineering*, Copenhagen, Denmark, 169–176.
- Zhou, Y., Kareem, A., and Gu, M. (2000). "Equivalent static buffeting loads on structures." *J. Struct. Eng.*, 126(8), 989–992.
- Tamura, Y., Kawai, H., Uematsu, Y., Marukawa, H., Fuji, K., and Taniiko, Y. (1996). "Wind load and wind-induced response estimations in RLB-AIJ1993." *Eng. Struct.*, 18(6), 399–411.
- Ho, T. C. E., Lythe, G. R., and Isyumov, N. (1999). "Structural loads and responses from the integration of instantaneous pressures." *Proc., 10th Int. Conf. on Wind Engineering*, Copenhagen, Denmark, 1505–1510.